

Title: Single spin-polarised Fermi surface in SrTiO₃ thin films

Authors: Eduardo B. Guedes^{1,2,*}, Stefan Muff^{1,2,*}, Mauro Fanciulli^{1,2}, Andrew P. Weber^{1,2}, Marco Caputo^{1,2}, Zhiming Wang⁴, Nicholas C. Plumb², Milan Radović², and J. Hugo Dil^{1,2}

Affiliations:

¹Institut de Physique,
École Polytechnique Fédérale de Lausanne,
CH-1015 Lausanne, Switzerland

²Photon Science Division,
Paul Scherrer Institut,
CH-5232 Villigen, Switzerland

³Key Laboratory of Magnetic Materials and Devices,
Ningbo Institute of Materials Technology and Engineering,
Chinese Academy of Sciences,
Ningbo 315201, Peoples Republic of China

(Dated: June 1, 2022)

Abstract

The 2D electron gas (2DEG) formed at the surface of SrTiO₃(001) has attracted great interest because of its fascinating physical properties and promise as a novel electronic platform, but up to now has eluded a stable way to tune its properties. Using angle-resolved photoemission spectroscopy with and without spin resolution we here show that the band filling can be controlled by growing thin SrTiO₃ films on SrTiO₃(001) substrates with different Nb doping levels. This results in a single spin-polarised 2D Fermi surface in a superconducting system, which can be used as platform for Majorana physics. Based on our results it can furthermore be concluded that the 2DEG does not extend more than 3 unit cells into the film and that its properties are determined by the dielectric response of the system.

* These authors contributed equally

One sentence summary: The band filling of the 2D electron gas can be controlled by growing thin SrTiO₃ films on SrTiO₃(001) substrates with different Nb doping levels, resulting in a single spin-polarised 2D Fermi surface which, combined with its superconducting properties, makes SrTiO₃ a platform for Majorana physics.

Main text: Transition metal oxides are expected to play an important role in next generation electronics and devices, primarily driven by the interplay of lattice, charge, orbit, and spin degrees of freedom in these materials in combination with correlation effects (1). A prominent sub-class are the titanates with a perovskite structure (ATiO₃) which, despite having a large band gap in the bulk, at interfaces with other materials (or vacuum), develops a high mobility two-dimensional electron gas (2DEG) with a wide variety of intriguing properties (2–5). Especially SrTiO₃ has been extensively studied, partly because it was the first system where such a 2DEG was observed and partly because it is an easily accessible material.

Angle-resolved photoemission spectroscopy (ARPES) is the most direct technique to access the electronic structure of materials. From comparison of experiments using soft X-ray and VUV radiation it has become clear that there is a close connection between 2DEGs found at interfaces and those found at surfaces, although the different environment will cause subtle differences in the electronic structure (6, 7, and references therein). In summary, the 2DEG consists of two circular mainly $3d_{xy}$ -derived states with clear 2D characteristics and low effective mass ($m^* = 0.65m_e$), and ellipsoidal $3d_{xz}$ - and $3d_{yz}$ -derived states with much higher effective mass ($m^* = 15m_e$) and 3D-like dispersion (Fig. 1A). The formation of the 2DEG is most likely related to oxygen vacancies, structural distortions, and a confining potential at the surface, while its population is strongly dependent on light-induced effects (8–10).

Another promising aspect of the systems described above has been the discovery of a gate-tuneable Rashba-type effect with a Rashba parameter $\alpha = 3.4 \times 10^{-12}$ eVm for the 2DEG at LaAlO₃/STO (LAO/STO) interface (11), while LaTiO₃/STO interfaces have shown a larger splitting of 1.8×10^{-11} eVm (12). For the 2DEG at the SrTiO₃(001) surface an even larger $\alpha = 5 \times 10^{-11}$ eVm was found by spin- and angle-resolved photoemission spectroscopy (SARPES) (13). The latter shows a helical Rashba-like spin texture in addition to a Zeeman gap around the surface Brillouin zone (SBZ) centre. The exact nature of this observation and the relative contributions of magnetic order and spin-orbit interaction are still under

debate (14, 15), but the lifting of the degeneracy for the d_{xy} -derived states is clear both in experiment and theory.

The presence of both Rashba and Zeeman interactions leads to a spin gap Δ at the surface Brillouin zone (SBZ) centre of STO (Fig. 1A), promising a wide range of functionalities depending on where the chemical potential is placed. An interesting scenario occurs when the chemical potential is placed inside the Zeeman gap, in which case the system would resemble the situation required to form Majorana fermions (16). Especially given the presence of superconductivity in both bulk STO (17) and STO interfaces (2, 3), a whole new realm of physics opens up based on the interplay of magnetism, spin-orbit interaction, and superconductivity in a single material.

As indicated above, much of the functionality relies on being able to shift the chemical potential while not altering other properties. In semiconductors and oxides a common approach is to use a gate voltage, but for the LAO/STO interface this is known to also change the magnitude of the Rashba-type splitting (11). Furthermore, it is unclear whether such an approach causes any shift in the surface 2DEG of STO(001). Remarkably, apart from the 2DEG generated by Al deposition (18), all published ARPES studies on the surface 2DEG show an almost identical band filling irrespective of the bulk doping level and whether the sample is prepared by cleaving (8, 9) or *in-situ* annealing (10), and of the amount of oxygen vacancies. This indicates that the origin of the 2DEG lies beyond a simple band bending picture, in which other ingredients such as structural distortions may also play a role. It should be noted that this behaviour is in stark contrast to anatase TiO_2 (19) or TiO_2 enriched surfaces of SrTiO_3 (20) in which the band filling can be tuned by the amount of oxygen vacancies.

In this work we follow a different and stable approach to tailor the chemical potential, namely the homoepitaxial growth of thin SrTiO_3 films on TiO_2 -terminated Nb-doped $\text{SrTiO}_3(001)$ substrates. Our main finding is that for films from 3 to at least 20 unit cells (u.c.) on 0.5 wt.% Nb-doped substrates the band filling is such that the Fermi level is exactly in the Zeeman gap at the SBZ centre, thus resulting in a single spin-polarised 2D Fermi surface (Fig. 1B). Further, we show that it is possible to change the position of the Fermi level by varying the amount of Nb dopants in the substrate. The similarities in the 2DEG found in films with different thicknesses indicate that the difference between single crystals and the films is not due to finite size effects, but due to a distinct dielectric response

of the system. This in turn is expected to change the properties of the polaronic excitations and thus the band characteristics.

The ARPES data for the 3, 5, and 20 u.c. STO films on 0.5 wt% Nb-doped STO substrate shows marked differences to the data typically obtained for STO single crystals (8–10), exhibiting only the d_{xy} -derived band for all photon energies used (Fig. S1A). On the other hand, the close comparison of the band structures of the STO films with different thicknesses shows very similar Fermi surfaces (Figs. 2, A to C) and band dispersions (Fig. 2, D to F) for all the three cases. There is no noticeable change regarding the Fermi wave vector k_F (Fig. 2J) and also the formation of the valence band (Figs. 2K) and the in-gap state (Figs. 2L) are similar for the three films. In the 2D curvature (21) (Figs. 2, G to I) and in the k_x integrated EDCs (Figs. 2M), polaron replicas of the d_{xy} band with an energy separation of ≈ 100 meV are visible. These are large polarons formed in the photoemission process commonly observed in titanates (19, 20). It is also worth noting the intense incoherent spectral weight at the center of the SBZ that appears below 150 meV, also often observed for the 2DEG on STO crystals (8–10). The fact that no differences are observed as a function of film thicknesses rules out the influence of finite size effects and constrains the spatial extension of this 2DEG from the top TiO_2 layer to 2 u.c. or less into the film. The 2D curvature data shows the shape of the d_{xy} band that follows a free-electron-like dispersion. The parabola plotted in Figs. 2 F and I, with a band bottom of 80 meV and an effective mass of $m^*=0.74m_e$ matches well the observed dispersion of the three samples. The small increase in effective mass ($m^*=0.65m_e$ for the 2DEG on STO single crystals (10)) points to an altered bond angle, likely due to surface relaxation. Due to the absence of the heavy d_{xz}/d_{yz} bands, it cannot be confirmed whether the splitting between the latter and the d_{xy} band has changed.

Apart from the small change in bond angle, the most striking difference of the 2DEG found on our STO/Nb:STO films when compared to the universal 2DEG found in cleaved and annealed STO crystals (8–10) is the large reduction of band filling from 230 to 80 meV, which corresponds to a downwards shift of the Fermi level. As will be explained below, this shift can be associated with a change in the dielectric properties of the system. Optical and spectroscopic measurements have shown that the dielectric response of SrTiO_3 changes from single crystals to thin films (22, 23). In addition, the in-gap states observed in our thin films are different from the ones observed in the bulk counterpart (Figs. 2M). For single

crystal STO (dashed line) two in-gap states are observed whereas for the STO films the state at 2.5 eV binding energy has disappeared. Both in-gap states are known to originate from defects (24, 25). Although the exact nature of the defects is still under debate, it is commonly accepted that they cause structural distortions, around which localised electronic states are formed, which can be regarded as small polarons. The different in-gap states clearly indicate a different defect structure, which results in an altered dielectric response of our PLD grown STO films when compared to STO crystals.

Of importance to the 2DEG characteristics is how the change in dielectric properties will influence the system's response to polar instabilities, given that undoped STO is an incipient ferroelectric material (26). In fact, it was shown that at the surface of cleaved $\text{KTaO}_3(001)$, metallization arises as a response to polar instabilities (27). Additionally, polarons have been proposed to drive the surface reconstruction in TiO_2 (28). More recently, the superconducting transition temperature in a FeSe monolayer grown on STO was shown to be raised after photoexcitation of the SrTiO_3 substrate, which was attributed to metastable polar distortions at the FeSe/ SrTiO_3 interface (29). Further, the mechanism underlying the writing of conductive paths in the LAO/STO interface by a metallic tip is attributed to a local polar distortion at the interface (30). All of the aforementioned experimental evidences suggest that the properties of the 2DEG are intimately connected to the dielectric response of the surface layer.

Extrapolating from the point-like defects responsible for small polarons, the breaking of translation symmetry at the surface of the sample can be considered as a 2D defect, which will trigger polar lattice distortions. Charges originating from photoexcitation or from oxygen vacancies act in order to minimize the surface free energy, thus screening the polar instability and giving rise to the 2DEG. The 2DEG can then be regarded as a "frozen polaron", *i.e.* charges coupled to static polar lattice distortions. The polar response to the defects and the efficiency of the screening, and thus the details of the 2DEG, depend on the dielectric response of the system, which is different in the films compared to crystals.

Regardless of the exact origin of the change in band filling observed in our films, it result in only a single band crossing the Fermi level (Figs. 2). Considering the spin texture measured for the 2DEG on the surface of bulk STO (13), applying a rigid upwards energy shift would lead to a single spin-polarized Fermi surface. However, given the general differences of thin films, a change in spin splitting cannot be excluded and requires experimental verification.

In order to access this often elusive degree of freedom, we employed spin-resolved ARPES to study 10 u.c. STO/Nb:STO films, well within the previously studied 3–20 u.c. range.

Fig. 3A shows the spin-integrated band dispersion measured with COPHEE for such a film on 0.5 wt% Nb:STO along the $\overline{\Gamma Y}$ direction, with 85 eV, circularly polarised photons. The dashed blue line represents the same band dispersion as in Fig. 2. The respective spin-resolved MDC measured at the Fermi level is shown in Fig. 3B. The main spin polarisation signal points along the x -direction, while the measured out-of-plane spin polarisation is most likely due to spin interference during the photoemission process (31) and $|P_y| \leq 0.04$ (Fig. S6, A to C).

A well-established routine (32) was used to simultaneously fit the total intensities and the spin polarisation vector. The fitted total intensity and polarisation along the sample x direction (P_x) are represented by green solid lines in Figs. 3B, while the red and blue dashed lines represent the individual peaks of the fit. The spectrum around $\overline{\Gamma_{10}}$ originates from a single band whose polarisation is perpendicular to the crystal momentum and reverses sign at the SBZ centre, consistent with a helical spin texture as also observed for the 2DEG on STO crystals (13). Hence, the Fermi level for the films grown on 0.5 wt% Nb-doped STO(001) substrate (Fig. 2) lies inside the Zeeman gap and the electronic structure thus show a single spin-polarised Fermi surface.

To be able to utilise the full potential of this material, it has to be possible to manipulate its properties by external means. In order to simulate the the change in carrier density by gating of the STO substrate, we have grown films on STO wafers where the amount of Nb dopants is changed by one order of magnitude; *i.e.* 10 u.c. STO film grown on a TiO₂ terminated, 0.05 wt% Nb-doped STO(001) substrate. Similarly, this film also hosts a purely 2D state (Fig. S4, A and B), but in this case the d_{xy} -derived band is more populated, and an inner band is now visible at lower binding energies. Figs. 3C show the spin-integrated ARPES data measured with $h\nu=85$ eV, circularly polarised light along the $\overline{\Gamma Y}$ directions. The dashed lines represent electron-like dispersions with the same effective mass as in Fig. 2, however with band bottoms of 170 meV and 50 meV, corresponding to a rigid band shift of 90 meV compared to the films grown on the 0.5 wt% Nb-doped substrate (Fig. S5, A to C). The spin-resolved MDC of the film grown on the 0.05 wt% Nb-doped substrate is displayed in Fig. 3D, also measured at the Fermi level. The data clearly shows two bands that reverse sign at zone center and are oppositely polarised, suggesting that the inner band

is the Rashba pair of the outer one. Thus, changing the substrate doping causes a change in band topology because the Fermi level moves above the Zeeman gap.

That reducing the amount of Nb dopants in the substrate leads to a surface 2DEG with increased band filling also indicates that the 2DEG is directly affected by the dielectric response of STO. In turn, the latter depends on the metallicity of the environment (33). In other words, the charges provided by the Nb dopants alter the boundary conditions and the dielectric response of the films, thus changing the band filling of the 2DEG. Note that this shift is in the opposite direction as would be expected by a simple model where the additional charges from Nb doping change the band filling. Interestingly, the film grown on the 0.5% substrate is such that the chemical potential lies inside the Zeeman gap, leading to a single spin-polarised band (Fig. 1B). In practice, this result means that local gating of the substrate can be used to create wires at whose tips zero bias anomalies should be observable by tunnelling experiments. Alternatively the wires can also be written by illuminating with an intense light source, by local defect doping, or by writing with a conductive tip (30). In combination with the superconducting properties of STO, this unifies all the ingredients for the formation of Majorana fermions in a single material without the need of external fields.

REFERENCES AND NOTES

- [1] N. Spaldin, S.-W. Cheong, and R. Ramesh, *Physics Today* **63**, 38 (2010).
- [2] N. Reyren, S. Thiel, A. D. Caviglia, L. F. Kourkoutis, G. Hammerl, C. Richter, C. W. Schneider, T. Kopp, A.-S. Rüetschi, D. Jaccard, M. Gabay, D. A. Muller, J.-M. Triscone, and J. Mannhart, *Science* **317**, 1196 (2007).
- [3] J. A. Bert, B. Kalisky, C. Bell, M. Kim, Y. Hikita, H. Y. Hwang, and K. A. Moler, *Nature Physics* **7**, 767 (2011).
- [4] Ariando, X. Wang, G. Baskaran, Z. Q. Liu, J. Huijben, J. B. Yi, A. Annadi, A. R. Barman, A. Rusydi, S. Dhar, Y. P. Feng, J. Ding, H. Hilgenkamp, and T. Venkatesan, *Nature Communications* **2**, 188 (2011).
- [5] B. Kalisky, J. A. Bert, C. Bell, Y. Xie, H. K. Sato, M. Hosoda, Y. Hikita, H. Y. Hwang, and K. A. Moler, *Nano Letters* **12**, 4055 (2012).
- [6] N. C. Plumb and M. Radović, *Journal of Physics: Condensed Matter* **29**, 433005 (2017).

- [7] E. Frantzeskakis, T. C. Rödel, F. Fortuna, and A. F. Santander-Syro, *Journal of Electron Spectroscopy and Related Phenomena* **219**, 16 (2017).
- [8] A. F. Santander-Syro, O. Copie, T. Kondo, F. Fortuna, S. Pailhès, R. Weht, X. G. Qiu, F. Bertran, A. Nicolaou, A. Taleb-Ibrahimi, P. L. Fèvre, G. Herranz, M. Bibes, N. Reyren, Y. Apertet, P. Lecoeur, A. Barthélémy, and M. J. Rozenberg, *Nature* **469**, 189 (2011).
- [9] W. Meevasana, P. D. C. King, R. H. He, S.-K. Mo, M. Hashimoto, A. Tamai, P. Songsiriritthigul, F. Baumberger, and Z.-X. Shen, *Nature Materials* **10**, 114 (2011).
- [10] N. C. Plumb, M. Salluzzo, E. Razzoli, M. Månsson, M. Falub, J. Krempasky, C. E. Matt, J. Chang, M. Schulte, J. Braun, H. Ebert, J. Minár, B. Delley, K.-J. Zhou, T. Schmitt, M. Shi, J. Mesot, L. Patthey, and M. Radović, *Phys. Rev. Lett.* **113**, 086801 (2014).
- [11] A. D. Caviglia, M. Gabay, S. Gariglio, N. Reyren, C. Cancellieri, and J.-M. Triscone, *Physical Review Letters* **104**, 126803 (2010).
- [12] M. J. Veit, R. Arras, B. J. Ramshaw, R. Pentcheva, and Y. Suzuki, *Nature Communications* **9**, 1458 (2018).
- [13] A. F. Santander-Syro, F. Fortuna, C. Bareille, T. C. Rödel, G. Landolt, N. C. Plumb, J. H. Dil, and M. Radović, *Nature materials* **13**, 1085 (2014).
- [14] L. P. Gor'kov, *Journal of Physics: Condensed Matter* **27**, 252001 (2015).
- [15] S. McKeown Walker, S. Riccò, F. Y. Bruno, A. de la Torre, A. Tamai, E. Golias, A. Varykhalov, D. Marchenko, M. Hoesch, M. S. Bahramy, P. D. C. King, J. Sánchez-Barriga, and F. Baumberger, *Physical Review B* **93**, 245143 (2016).
- [16] V. Mourik, K. Zuo, S. M. Frolov, S. R. Plissard, E. P. A. M. Bakkers, and L. P. Kouwenhoven, *Science* **336**, 1003 (2012).
- [17] J. F. Schooley, W. R. Hosler, and M. L. Cohen, *Phys. Rev. Lett.* **12**, 474 (1964).
- [18] T. C. Rödel, F. Fortuna, S. Sengupta, E. Frantzeskakis, P. L. Fèvre, F. Bertran, B. Mercey, S. Matzen, G. Agnus, T. Maroutian, P. Lecoeur, and A. F. Santander-Syro, *Advanced Materials* **28**, 1976 (2016).
- [19] S. Moser, L. Moreschini, J. Jaćimović, O. S. Barišić, H. Berger, A. Magrez, Y. J. Chang, K. S. Kim, A. Bostwick, E. Rotenberg, L. Forró, and M. Grioni, *Phys. Rev. Lett.* **110**, 196403 (2013).
- [20] Z. Wang, S. M. Walker, A. Tamai, Y. Wang, Z. Ristic, F. Y. Bruno, A. De La Torre, S. Riccò, N. Plumb, M. Shi, P. Hlawenka, J. Snchez-Barriga, A. Varykhalov, T. Kim, M. Hoesch,

- P. King, W. Meevasana, U. Diebold, J. Mesot, B. Moritz, T. Devereaux, M. Radović, and F. Baumberger, *Nature materials* **15**, 835 (2016).
- [21] P. Zhang, P. Richard, T. Qian, Y.-M. Xu, X. Dai, and H. Ding, *Review of Scientific Instruments* **82**, 043712 (2011).
- [22] A. A. Sirenko, C. Bernhard, A. Golnik, A. M. Clark, J. Hao, W. Si, and X. X. Xi, *Nature* **404**, 373 (2000).
- [23] T. Ostapchuk, J. Petzelt, V. Železný, A. Pashkin, J. Pokorný, I. Drbohlav, R. Kužel, D. Rafaja, B. P. Gorshunov, M. Dressel, C. Ohly, S. Hoffmann-Eifert, and R. Waser, *Phys. Rev. B* **66**, 235406 (2002).
- [24] Y. S. Kim, J. Kim, S. J. Moon, W. S. Choi, Y. J. Chang, J.-G. Yoon, J. Yu, J.-S. Chung, and T. W. Noh, *Applied Physics Letters* **94**, 202906 (2009).
- [25] S. A. Chambers, Y. Du, Z. Zhu, J. Wang, M. J. Wahila, L. F. J. Piper, A. Prakash, J. Yue, B. Jalan, S. R. Spurgeon, D. M. Kepaptsoglou, Q. M. Ramasse, and P. V. Sushko, *Phys. Rev. B* **97**, 245204 (2018).
- [26] K. A. Müller and H. Burkard, *Phys. Rev. B* **19**, 3593 (1979).
- [27] M. Setvin, M. Reticcioli, F. Poelzleitner, J. Hulva, M. Schmid, L. A. Boatner, C. Franchini, and U. Diebold, *Science* **359**, 572 (2018).
- [28] M. Reticcioli, M. Setvin, X. Hao, P. Flauger, G. Kresse, M. Schmid, U. Diebold, and C. Franchini, *Phys. Rev. X* **7**, 031053 (2017).
- [29] M. Yang, C. Yan, Y. Ma, L. Li, and C. Cen, *Nature Communications* **10**, 85 (2019).
- [30] C. Cen, S. Thiel, G. Hammerl, C. Schneider, K. Andersen, C. Hellberg, J. Mannhart, and J. Levy, *Nature Materials* **7**, 298 (2008).
- [31] J. H. Dil, *Electronic Structure* **1**, 023001 (2019).
- [32] F. Meier, J. H. Dil, and J. Osterwalder, *New Journal of Physics* **11**, 125008 (2009).
- [33] Z. Yu and C. Ang, *Applied Physics Letters* **80**, 643 (2002), <https://doi.org/10.1063/1.1435409>.
- [34] K. Momma and F. Izumi, *Journal of Applied Crystallography* **44**, 1272 (2011).

ACKNOWLEDGMENTS

This work was financially supported by the Swiss National Science foundation (SNF) Project No. PP00P2_144742 and No. PP00P2_170591.

SUPPLEMENTARY MATERIALS

Materials and methods

References S1, S5

Figs. S1 to S6

Fig. 1

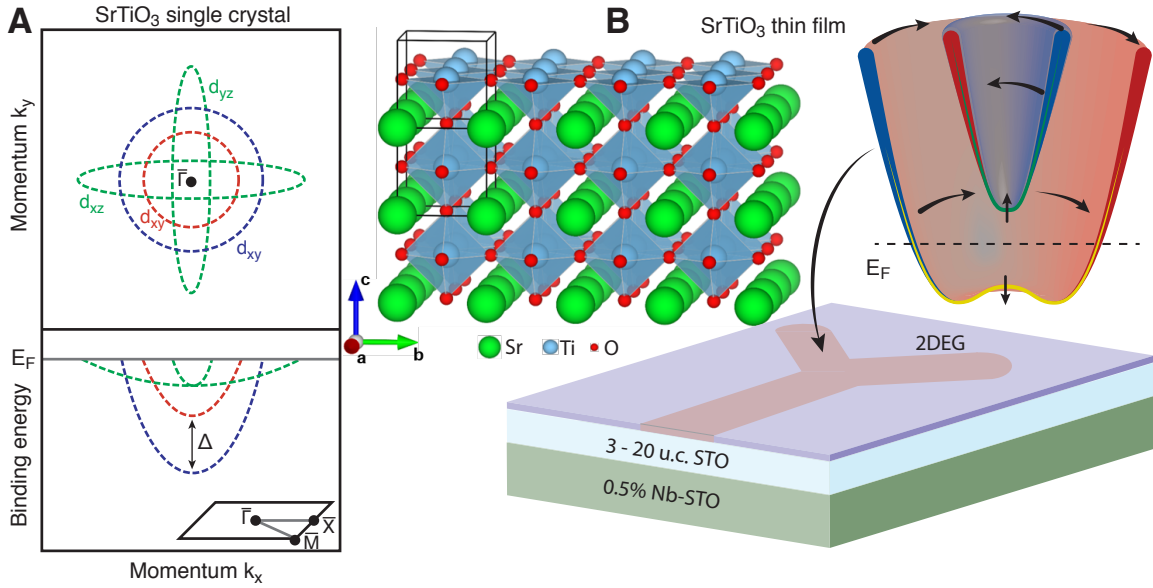


FIG. 1. The spin-polarised 2DEG on SrTiO₃ crystals and thin films. (A) Schematics of the electronic structure of the 2DEG on STO crystals, consisting of two circular $3d_{xy}$ -derived states (red and blue) and ellipsoidal $3d_{xz}$ - and $3d_{yz}$ -derived states (green). The inset shows the surface cubic Brillouin Zone. (B) Illustration showing the crystal structure (\mathcal{A}_4) of STO and the STO film grown on 0.5 wt% Nb-doped STO substrate, along with the band structure of the hosted 2DEG. In this case, the Fermi level lies in the Zeeman gap at the SBZ centre, thus resulting in a single spin-polarised 2D Fermi surface. This band structure, along with the superconducting properties of STO, makes this material a 2D Majorana platform.

Fig. 2

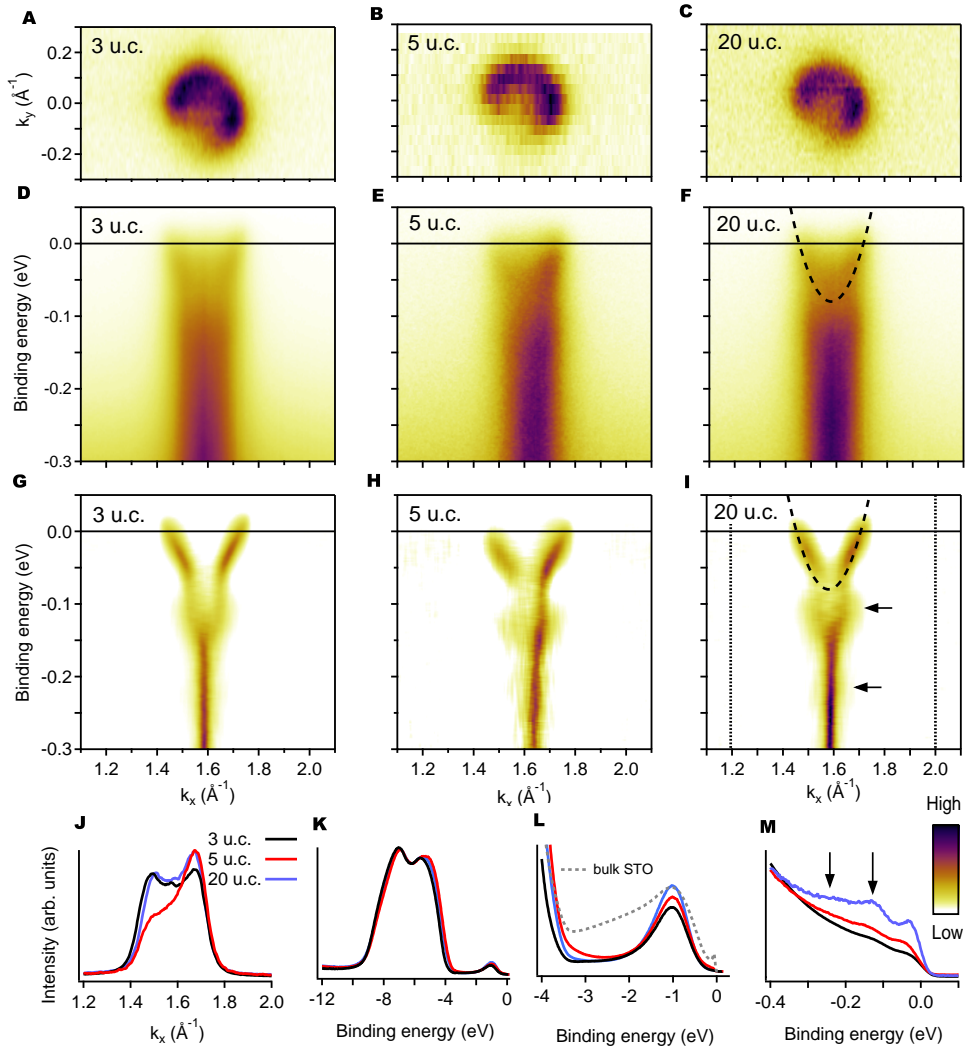


FIG. 2. **Detailed spectroscopy of single Fermi sheet.** (A) Fermi surface, (B) band structure and (G) 2D curvature for 3 u.c. STO on the 0.5 wt% Nb-doped substrate at $\overline{\Gamma_{01}}$ with $h\nu=85$ eV (C^+). (B,E,H) and (C,F,I) same as (A,D,G) but for 5 u.c. and 20 u.c. respectively. A free electron like parabola is indicated in (F,I). (J) MDCs of the three films at the Fermi energy from (D,E,F). k_x integrated EDCs of the valence band (K), the in-gap state (L), and close to the Fermi energy (M) with indicated polaron replicas (black arrows). In (L) the spectrum of a STO single crystal is shown for comparison.

Fig. 3

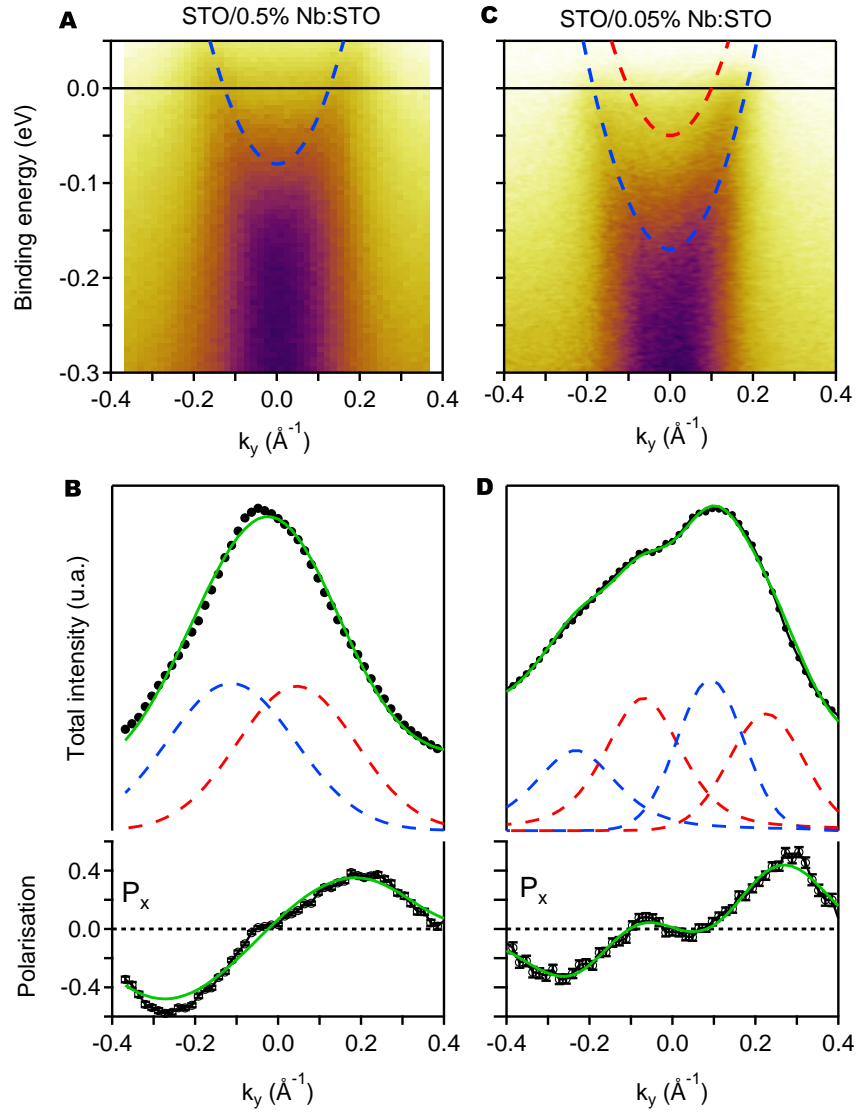


FIG. 3. Single spin-polarised band and shift of Fermi level. (A) Electron dispersion of 10 u.c. STO film grown on 0.5 wt% Nb:STO and (C) on 0.05 wt% Nb:STO. (B) Spin-resolved MDCs at the Fermi level [indicated in A and C] and respective P_x spin polarisation of the 10 u.c. STO film grown on 0.5 wt% Nb:STO film and (D) on 0.05 wt% Nb:STO film. The solid green lines are results of fits with (B) two and (D) four peaks.

Supplementary information for “Single spin-polarised Fermi surface in SrTiO₃ thin films”

Eduardo B. Guedes^{1,2,*}, Stefan Muff^{1,2,*}, Mauro Fanciulli^{1,2}, Andrew P. Weber^{1,2}, Marco Caputo^{1,2}, Zhiming Wang³, Nicholas C. Plumb², Milan Radović², and J. Hugo Dil^{1,2}

¹*Institut de Physique,*

École Polytechnique Fédérale de Lausanne,

CH-1015 Lausanne, Switzerland

²*Photon Science Division,*

Paul Scherrer Institut,

CH-5232 Villigen, Switzerland

³*Key Laboratory of Magnetic Materials and Devices,*

Ningbo Institute of Materials Technology and Engineering,

Chinese Academy of Sciences,

Ningbo 315201, Peoples Republic of China

(Dated: June 1, 2022)

* These authors contributed equally

This PDF file includes:

Methods

Supplementary Text

Figs. S1 to S6

METHODS

The SrTiO₃ thin films were grown by pulsed laser deposition (PLD) on commercially available, single TiO₂ terminated 0.05 and 0.5 wt% Nb-doped STO(001) substrates (Twente Solid State Technology), using a crystalline STO disk as target, as will be described below. The prepared films were transferred *in-situ* to the high-resolution ARPES endstation at the Surface and Interface Spectroscopy beamline of the Swiss Light Source at the Paul Scherrer Institut. X-ray photoemission (XPS) and ARPES spectra were measured with a Scienta R4000 analyzer with instrumental angle and energy resolution better than 0.2° and 10 meV. In order to perform spin-resolved ARPES, new films were grown and transferred in a vacuum suitcase under ultra-high vacuum conditions to the COPHEE endstation [S1], which uses an Omicron EA 125 hemispherical energy analyser and two orthogonally assembled classic Mott detectors. The angle and energy resolutions of the SARPES measurements are better than 1.5° and 70 meV. For all the measurements the samples were kept under pressures better than 5×10^{10} mbar and at 20 K. No further sample treatment was required. These results were reproduced on different samples, in independent experiments.

SUPPLEMENTARY TEXT

Growth of the films

The SrTiO₃ thin films were grown by pulsed laser deposition (PLD) on commercially available, single TiO₂ terminated 0.05 and 0.5 wt% Nb-doped STO(001) substrates (Twente Solid State Technology), using a crystalline STO disk as target. The reflection high-energy electron diffraction (RHEED) oscillations used to control the thicknesses of 3, 5, and 20 u.c. films on 0.5 wt% Nb-doped STO(001) are displayed in Fig. S1, A to C. The RHEED patterns recorded after the growth show straight lines indicating a flat, 2D film surface. Between the main diffraction intensities, low intensity lines are visible (Fig. S1, D to F). It

is interesting to note that the RHEED intensity actually increases with the growth of the first overlayer of STO on the substrate, indicating the high quality of the films.

Fermi surface, photon energy and polarisation dependence

The ARPES data for the 3, 5, and 20 u.c. STO films on 0.5 wt% Nb-doped STO substrate shows marked differences to the data typically obtained for STO single crystals[S2–S4]. In the data obtained for the films (Fig. S2, A to C) a circular Fermi surface is observed around the Γ points and there is no signature of the ellipsoidal d_{xz} - and d_{yz} -derived states for any of the three film thicknesses. In the photon energy scans of the 5 u.c. film (Fig. S2, D and E) the d_{xy} -derived state shows a pure 2D character, also observed for the 3 and 20 u.c. films as noted below. The observed intensity variations are due to the $3p$ – $3d$ resonance at around $h\nu = 45$ eV ($k_z \approx 3.8 \text{ \AA}^{-1}$) and Bloch spectral enhancement at bulk Γ points[S5]. Furthermore, surface reconstructions are visible in all the Fermi surfaces with varying clarity. The bands around the reconstructed $\bar{\Gamma}$ points are relatively featureless and (Fig. S2E), apart from a resonant enhancement do not show the same structure as a function of photon energy as the main $\bar{\Gamma}$ points. Therefore it appears that the reconstruction is not long range ordered and thus was not considered in the analysis.

The photon energy scans (*i.e.* dispersion along k_z , calculated using an inner potential $V_0 = 14.5$ eV[S4]) measured with circularly polarised light for 20 u.c. film on 0.5 wt% Nb-doped STO(001) around $\bar{\Gamma}_{00}$ and $\bar{\Gamma}_{10}$ (Fig. S3, A and B), confirm the absence of heavy bands (d_{xz} - and d_{yz} -derived). That the 2DEG is d_{xy} -derived can be seen by dependence of the Fermi surface with light polarisation (linear vertical and horizontal, LV and LH), which in our experimental geometry is a signature of a band with d_{xy} character (Fig. S3, C and D). For the 3 u.c. film there is no sign of the heavy bands at 85 eV (Fig. 2, A, D and G of main text), which is the typical energy at which these states are expected to appear in STO crystals[S4]. Hence an identical, purely d_{xy} -derived 2D state, is observed for the 3, 5 and 20 u.c. films. Similarly, for the the 10 u.c. film on the 0.05% Nb:STO substrate, the photon energy dependence measured around $\bar{\Gamma}_{00}$ and $\bar{\Gamma}_{10}$ with circularly polarised light (S4) show no sign of the heavy bands.

Detailed characterisation of film grown on low doped substrate

Fig. S5, A to C, shows ARPES data with $h\nu=47$ eV, LV-polarised light, obtained for a 10 u.c. STO film grown on a TiO_2 terminated, 0.05 wt% Nb-doped STO(001) substrate. Despite also hosting a purely 2D d_{xy} -derived state, its Fermi surface (Fig. S5A) shows an increase in intensity towards the center, indicating the presence of another band. This is confirmed by the band dispersion and its respective 2D curvature analysis (Figs.S5 B and C), from which it is clear that the d_{xy} -derived band has shifted to higher binding energy and that an inner band appears at low binding energies. The black dashed lines represent electron-like dispersions with the same effective mass as in Fig. 2 of the main text, but with band bottoms of 170 meV and 50 meV. The good match with the experimental data indicates a rigid band shift of 90 meV compared to the films grown on the 0.5 wt% Nb-doped substrate. The inner band has $k_F=0.07 \text{ \AA}^{-1}$, while k_F of the outer d_{xy} band has changed from 0.13 \AA^{-1} to 0.20 \AA^{-1} . These values are in agreement with the Fermi surface on Fig. S5A, in which the radius of the circles match the fitted values of k_F . Finally, it can be seen in the 2D curvature analysis that the well-defined polaron replicas on Fig. 2 of the main text evolved into kinks in the electron dispersion on Fig. S5C. As seen in anatase TiO_2 [S6] and TiO_2 enriched surfaces of SrTiO_3 [S7], this evolution signals the crossover from a polaronic to a short-ranged electron-phonon coupled state due to an increased carrier density.

SARPES analysis

Fig. S6 shows the band dispersion measured at the COPHEE endstation with $h\nu = 47$ eV, vertically polarised light for a 10 u.c. film on 0.05 wt% Nb-doped STO(001). The good match with the parabolas from Fig. 3C of the main text validates the quality of the film transferred to the COPHEE endstation and, more importantly, of the measurements performed in this endstation. In turn, the total intensity of the MDCs measured around $E_{1,2}$ (defined in Fig. S6A, where the rectangles represent the 70 meV energy resolution) and related spin polarisation curves along k_y are shown in Fig. S6, B and C. For both $E_{1,2}$ the main spin polarisation signal is along the x -direction, consistent with a Rashba-type splitting, while the measured out-of-plane spin polarisation is most likely due to spin interference during the photoemission process[S8] and $|P_y| \leq 0.04$. A well-established routine[S9] was used to

simultaneously fit the total intensities and the spin polarisations along the sample x-, z-, and y-axis for $E_{1,2}$, represented by green solid lines in Fig. S6, B and C. For $E=E_1$ (Fig. S6B) two peaks with opposite spin polarisation result from the analysis, while the spectra measured around $E = E_2$ (Fig. S6C) can only be fitted assuming four peaks with alternating spin polarisation. The fitted peak positions are marked as red dots in Fig. S5B and match well with the high-resolution spectrum.

-
- [S1] M. Hoesch, T. Greber, V. N. Petrov, M. Muntwiler, M. Hengsberger, W. Auwaerter, and J. Osterwalder, *Journal of Electron Spectroscopy and Related Phenomena* **124**, 263 (2002).
- [S2] A. F. Santander-Syro, O. Copie, T. Kondo, F. Fortuna, S. Pailhès, R. Weht, X. G. Qiu, F. Bertran, A. Nicolaou, A. Taleb-Ibrahimi, P. L. Fèvre, G. Herranz, M. Bibes, N. Reyren, Y. Apertet, P. Lecoeur, A. Barthélémy, and M. J. Rozenberg, *Nature* **469**, 189 (2011).
- [S3] W. Meevasana, P. D. C. King, R. H. He, S.-K. Mo, M. Hashimoto, A. Tamai, P. Songsiriritthigul, F. Baumberger, and Z.-X. Shen, *Nature Materials* **10**, 114 (2011).
- [S4] N. C. Plumb, M. Salluzzo, E. Razzoli, M. Månsson, M. Falub, J. Krempasky, C. E. Matt, J. Chang, M. Schulte, J. Braun, H. Ebert, J. Minár, B. Delley, K.-J. Zhou, T. Schmitt, M. Shi, J. Mesot, L. Patthey, and M. Radović, *Phys. Rev. Lett.* **113**, 086801 (2014).
- [S5] J. H. Dil, J. W. Kim, S. Gokhale, M. Tallarida, and K. Horn, *Phys. Rev. B* **70**, 045405 (2004).
- [S6] S. Moser, L. Moreschini, J. Jaćimović, O. S. Barišić, H. Berger, A. Magrez, Y. J. Chang, K. S. Kim, A. Bostwick, E. Rotenberg, L. Forró, and M. Grioni, *Phys. Rev. Lett.* **110**, 196403 (2013).
- [S7] Z. Wang, S. M. Walker, A. Tamai, Y. Wang, Z. Ristic, F. Y. Bruno, A. De La Torre, S. Riccò, N. Plumb, M. Shi, P. Hlawenka, J. Sanchez-Barriga, A. Varykhalov, T. Kim, M. Hoesch, P. King, W. Meevasana, U. Diebold, J. Mesot, B. Moritz, T. Devereaux, M. Radović, and F. Baumberger, *Nature materials* **15**, 835 (2016).
- [S8] J. H. Dil, *Electronic Structure* **1**, 023001 (2019).
- [S9] F. Meier, J. H. Dil, and J. Osterwalder, *New Journal of Physics* **11**, 125008 (2009).

Fig. S1

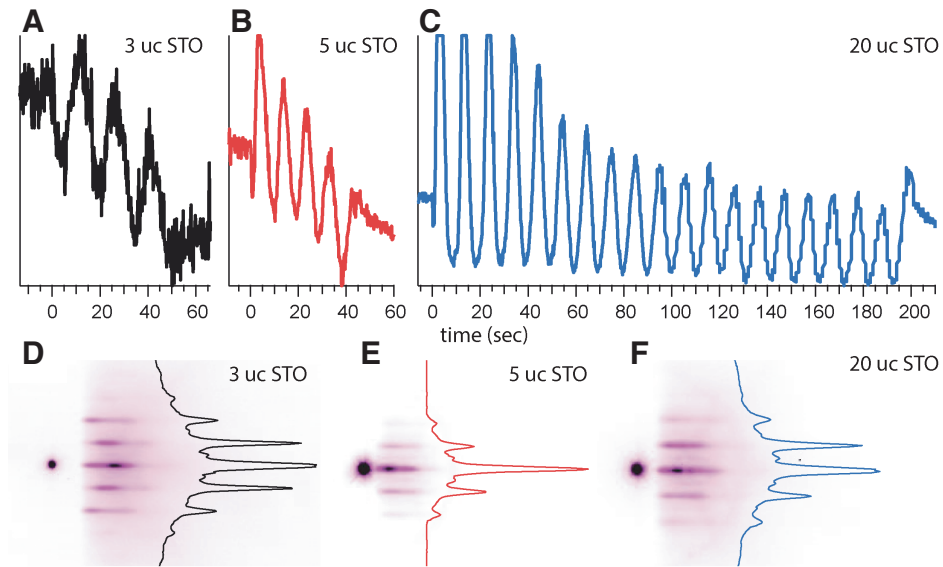


FIG. S1. **Growth of SrTiO_3 thin films on Nb-doped $\text{SrTiO}_3(001)$ substrate.** RHEED oscillations of the film growth of (A) 3 u.c., (B) 5 u.c. and (C) 20 u.c. STO on 0.5 wt% Nb:STO(001) substrates. (D-F) RHEED patterns of the three films after the growth at the growth temperature, along with the intensity line profiles.

Fig. S2

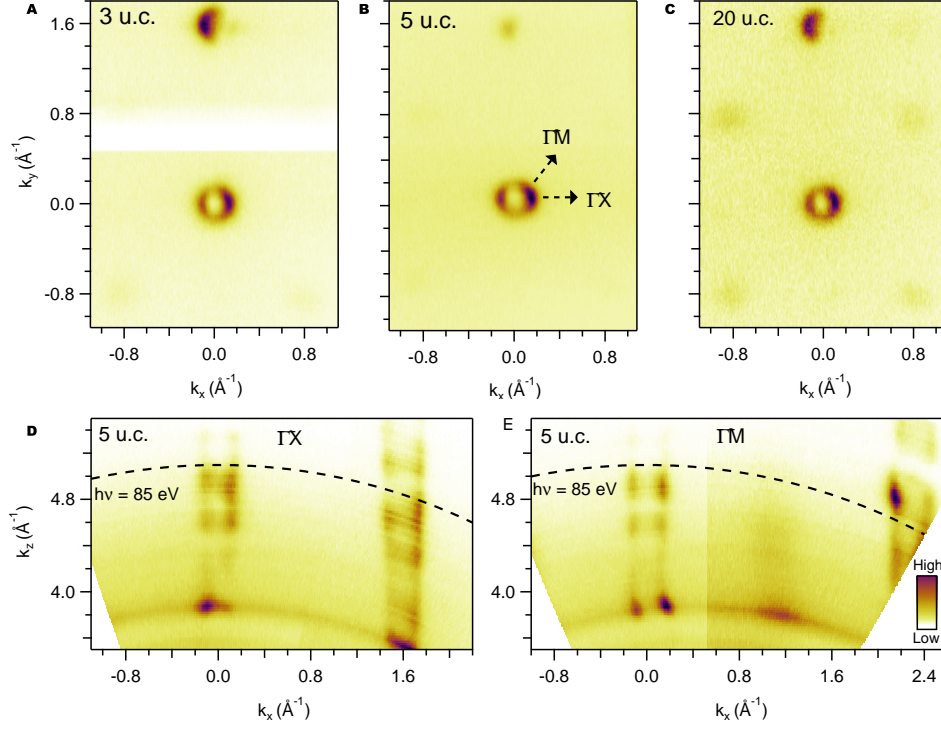


FIG. S2. **3D Fermi surface mapping of state at SrTiO₃ film surfaces.** (A-C) Fermi surface of 3, 5, and 20 u.c. thick films grown on the 0.5 wt% Nb-doped substrate, measured at $h\nu = 85 \text{ eV}$ with circularly polarised light (C^+) covering $\overline{\Gamma_{00}}$ and $\overline{\Gamma_{01}}$ as well as reconstructed Γ -points. The lack of signal in (A) at $k_y = 0.5 \text{\AA}^{-1}$ is due to a synchrotron beam loss. (D) Dispersion with k_z for the 5 u.c. sample along $\overline{\Gamma X}$ and (E) along $\overline{\Gamma M}$ as indicated in (B).

Fig. S3

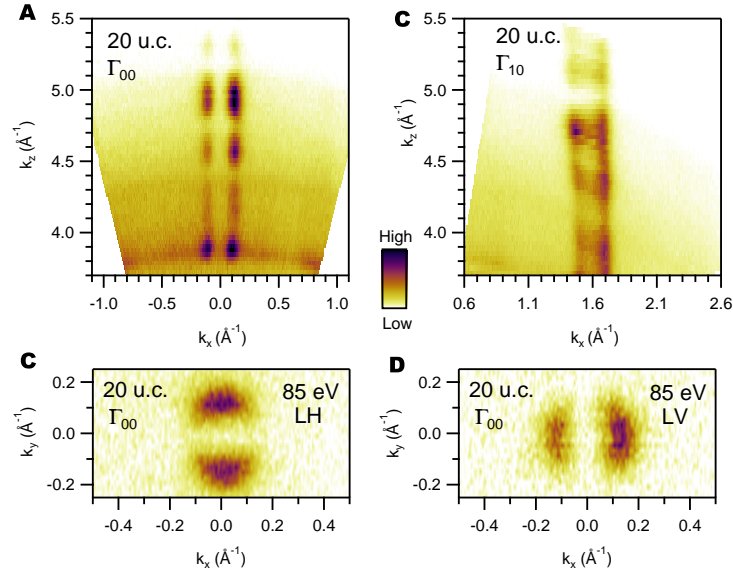


FIG. S3. The 2DEG on the 20 u.c. film on 0.5 wt% Nb-doped STO(001). Dispersion with k_z for the 20 u.c. sample around (A) $\overline{\Gamma_{00}}$ and (B) $\overline{\Gamma_{10}}$ confirms a purely 2D state. Fermi surfaces with different light polarisations confirm the d_{xy} character of the 2DEG.

Fig. S4

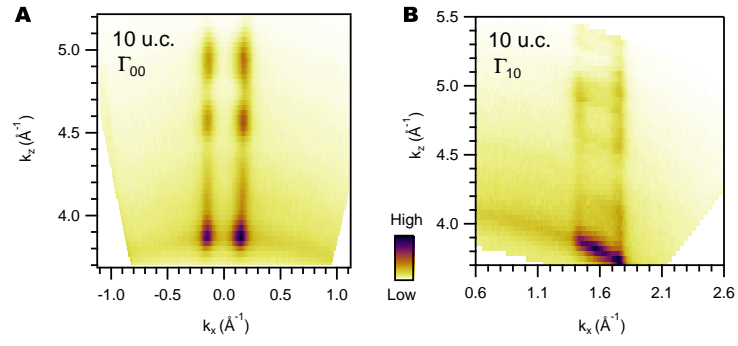


FIG. S4. **The 2DEG on the 10 u.c. film on 0.05 wt% Nb-doped STO(001).** Fermi surface in the $k_x - k_z$ plane for the 10 u.c. film on 0.05 wt% Nb-doped STO(001) around (A) $\overline{\Gamma_{00}}$ and (B) $\overline{\Gamma_{10}}$.

Fig. S5

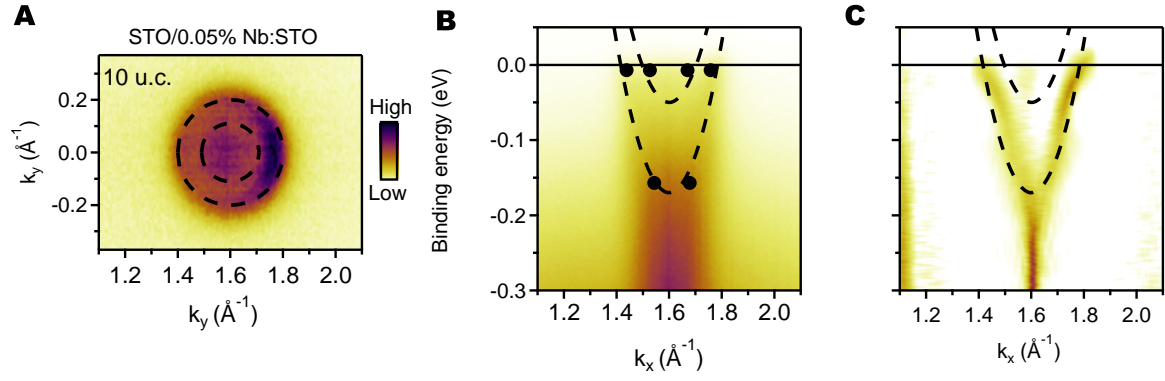


FIG. S5. Detailed 2DEG on the 10 u.c. film on 0.05 wt% Nb-doped STO(001). (A) Fermi surface measured with $h\nu = 47$ eV, LV-polarised light, with the band dispersion along (B) $\overline{\Gamma X}$ and (C) its 2D curvature plot.

Fig. S6

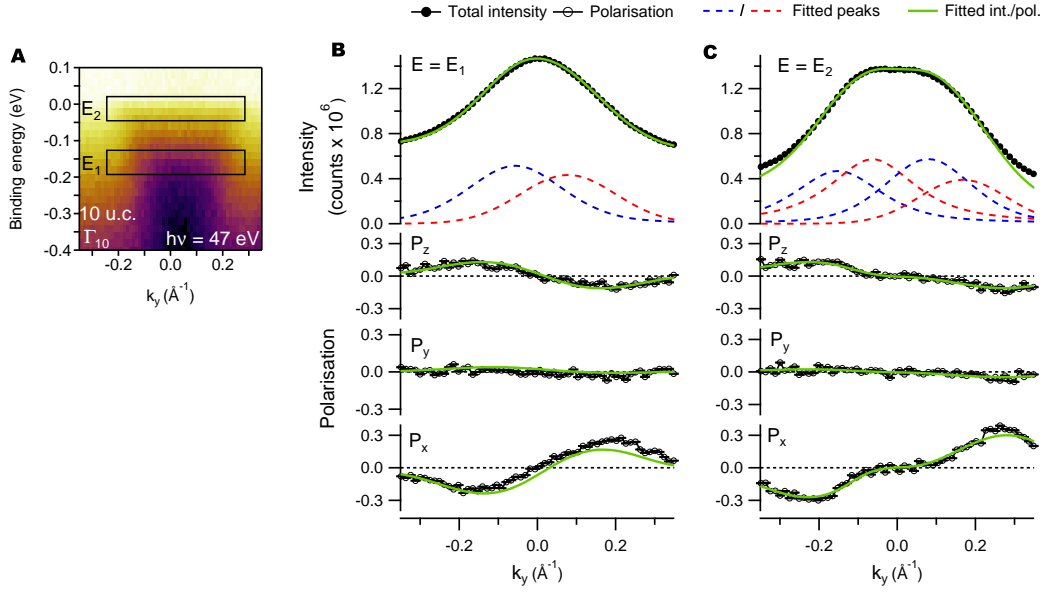


FIG. S6. Spin-polarisation of the 2DEG on a 10 u.c. film on 0.05 wt% Nb-doped STO(001). (A) Spin-integrated band map measured with $h\nu = 47$ eV, LV-polarised light, along with the parabolic dispersions used in Fig. 3C of the main text, and the definition of the $E_{1,2}$ energy windows. Total intensity and related $P_{x,y,z}$ spin polarisations, along with their respective fits for (B) $E = E_1$ and (C) $E = E_2$.